J. Math. Sci. Model., 8(1) (2025) 28-41 https://doi.org/10.33187/jmsm.1637233

Journal of Mathematical Sciences and Modelling

ISSN (Online) 2636-8692
https://dergipark.org.tr/en/pub/jmsm

Research Article

PI Controller Design for a 5-Phase Switched Reluctance Motor with Bipolar Excitation Segmental Rotor

Erdal Büyükbıçakcı

Sakarya University of Applied Sciences, Department of Computer Technologies, Sakarya, Türkiye, ror.org/01shwhq58

Article Info

Keywords: *Mathematical model, PI control, Segmental rotor, Switched reluctance motor, Two phase excitation*
2020 AMS: *49N05, 93C83*
Received: *10 February 2025*
Accepted: *22 March 2025*
Available online: *25 March 2025*

Abstract

Switched Reluctance Motors (SRMs) are a type of motor that converts electrical energy into mechanical energy using the variable reluctance principle in industry, electric vehicles, and renewable energy. However, due to the nonlinear characteristic of the magnetic circuit depending on the rotor position, the dynamic performance of SRMs varies according to the operating conditions and they need a powerful drive circuit and an advanced control algorithm for maximum torque and stable speed control. In this regard, our solution involves the implementation of a PI control algorithm in a novel ST-SRM configuration that has been previously documented and is distinct from the conventional SRM design, which features a 5-phase 10/8 pole segmental rotor and bipolar excitation. has been developed to enhance the motor's overall operating performance and boost energy efficiency. The rotor of this five-phase, 10/8 pole configuration motor is made of silicon steel sheet packs and a lightweight aluminium block, in which these packs are placed to reduce the motor weight. Thus, the magnetic flux follows a short-circuited path between neighbouring stator poles, preventing stray fluxes and increasing the torque generated per unit weight. Short magnetic flux loops are used by simultaneous excitation of two neighboring phases, which reduces core losses, minimizes torque fluctuations, and allows higher torque production. However, the mathematical model of the motor becomes more complex as the cooperation of two phases results in mutual inductances between the phases. In this study, the mathematical model of the ST-SRM in the state space is derived, and the equation set required to control the system is obtained. The developed driver circuit is designed in a dual microcontroller architecture to manage the dual-phase supply of the motor. In this configuration, the primary microcontroller governs the five-phase power circuit, while the secondary microcontroller executes the PI algorithm in response to the speed signal from the optical rotor position sensors and autonomously modifies the source voltage. The instantaneous voltage adjustment of the drive system enables the ST-SRM speed to be maintained at the reference value, contingent on the fluctuating load conditions, thereby enhancing stability and energy efficiency. Experimental studies have demonstrated the efficacy of the PI controller in maintaining motor speed at a target value despite variations in load and in effectively dampening deviations during speed transitions. The measured phase current waveforms exhibit significant overlap with the simulation results, thereby substantiating the accuracy of the mathematical model and control method. Instantaneous monitoring of quantities such as current and speed through the developed user interface reveals the satisfactory dynamic performance of the system and the reliability of the control algorithm. In conclusion, an innovative PI-controlled driving and monitoring system for ST-SRM has been designed and successfully implemented. Thanks to the integrated drive system, the stable operation of the motor under speed and load is ensured, and the user interface makes real-time monitoring of critical parameters possible.

Email address and ORCID number: **erdal@subu.edu.tr, 0000-0001-7276-741X**
Cite as "E. Büyükbıçakcı, *PI controller design for a 5 phase switched reluctance motor with bipolar excitation segmental rotor*, J. Math. Sci. Model., 8(1) (2025), 28-41"

1. Introduction

Switched reluctance motors (SRMs), which convert electrical energy into mechanical energy based on the principle of variable reluctance effect, are in the class of innovative electrical machines that offer advantages such as cost-effectiveness, high durability, and high energy efficiency [1]. These motors, which stand out with their high energy efficiency, were first proposed theoretically in the 19th century and became controllable in the 1960s with advances in the field of power electronics [2]. Especially since the 1980s, intensive research and development studies on SRMs have led to significant improvements in control methods, drive technologies, and motor efficiency [3]. Today, the main reasons why SRMs are preferred in different application areas, such as industrial applications, electric vehicles, and renewable energy systems, are their low maintenance costs, high reliability, and superior performance characteristics [4]. In the literature, it is emphasized that these motors are superior to other motor types in terms of efficiency advantages and cost-effectiveness, especially under variable load conditions [5]. The development of modern control algorithms and the integration of sensorless control technologies have further improved the performance of SRMs and enabled the use of these motors in a wider range of applications [6, 7].

However, recent studies on the basic design parameters and control strategies of SRMs have revealed important findings to optimize the dynamic performance and energy efficiency of the motor. In particular, the use of modern power electronics systems and advanced magnetic materials improves the accuracy of SRMs in electromagnetic moment generation and increases the competitiveness of these motors in applications requiring precise control. Therefore, because of sustainability goals and innovative approaches in energy conversion technologies, SRMs continue to be a research and development topic that attracts attention in academic and industrial fields.

Switched Reluctance Motors are increasingly used in modern industrial systems due to their low rotor losses and durable mechanical structures. These motors attract attention with their advantages such as energy efficiency and high moment density, especially in applications requiring variable speed and servo control [8, 9]. SRMs designed for electric vehicles significantly increase energy efficiency and environmental sustainability while reducing production costs [10, 11]. In space technologies, SRMs have become an ideal solution for satellite and spacecraft systems due to their simple low-maintenance design and ability to operate over wide temperature ranges [12]. In addition, SRMs have been shown to be used with energy-saving control algorithms in applications requiring high dynamic response, such as radar systems, automatic doors, and water pumps [13]. In household appliances, SRMs are widely used in applications such as washing machines and Heating, Ventilation, and Air Conditioning (HVAC) systems due to their structural durability and low serviceability [3, 14]. In rural areas, SRMs offer energy efficiency and low-cost advantages by providing easy integration with renewable energy sources in systems such as water pumps and agricultural machinery [3, 15]. With these versatile features, SRMs are widely used in industrial, domestic, and renewable energy applications.

Switched Reluctance Motors continue to be a subject of study for researchers due to the nonlinear characteristics of their magnetic circuits based on the relationship between phase currents and rotor position. This nonlinearity necessitates the implementation of advanced control algorithms that aim to efficiently minimize torque fluctuations with maximum torque production [1, 3, 16]. Advanced methods such as adaptive control strategies, Pulse Width Modulation (PWM), and hysteresis-based control techniques have been applied to optimize the efficiency of SRM [17, 18]. In addition, mathematical modelling of nonlinear magnetic structures and precise management of phase currents are very important in the design of highly efficient control systems. In this context, Büyükbıçakcı and Boz investigated in detail the mathematical equations of state and dynamic simulation results of a new type of bipolar-excited five-phase Segmental Rotor Switched Reluctance Motor (ST-SRM) [19]. This research contributes to the literature on the modelling of nonlinear characteristics of SRMs and the development of optimised control methods.

The ST-SRM has innovative features that significantly differentiate it from conventional SRM designs. In particular, the complete redesign of the rotor structure and the integration of bipolar excitation methods both increase the torque density and significantly improve the energy efficiency of these motors. In this context, the ST-SRM design developed by Uygun and Bal utilizes a segmental rotor structure, unlike conventional SRMs. This special structure allows for a more efficient orientation of the magnetic flux density, thereby increasing the torque generation capacity and significantly reducing torque fluctuations. The segmental rotor design also enables better management of inter-phase inductance effects, resulting in a balanced distribution of the generated torque [20]. This improves the overall dynamic performance of the motor and provides a more stable operation. This innovative ST-SRM design with bipolar excitation allows optimising the interphase magnetic flux interactions and reducing current losses. Especially when supported by modern control strategies, this design is expected to contribute to making SRM technology an attractive alternative for high efficiency applications.

ST-SRM based on segmental and bipolar excitation principles has attracted attention as an innovative research area that goes beyond conventional SRM designs. Extensive studies on motor design and drive circuits have been carried out to design the nonlinear magnetic properties of these motors and to control the current fluctuations under load. The first systematic research on SRMs was carried out by Lawrenson and Agu, which laid an important foundation for magnetic circuit optimization [21]. Mecrow and co-workers analyzed the performance parameters of SRMs with different pole and winding structures and revealed the effects of these structures on torque generation and speed stability [22]. Uygun and Bal developed a new U-type ST-SRM design performed linear modeling of the magnetic circuit of the motor, and emphasized the effects of segmental structures on torque generation [20]. Xu et al. compared the speed and torque performances of classical SRMs and ST-SRMs with different topology methods and emphasized the potential of segmental structures to increase energy efficiency [9].

In other studies, innovative topologies have been developed to optimize the pole, rotor and winding structures of SRMs. Research in this area has sought to mitigate energy dissipation and reduce torque ripples by manipulating magnetic flux distribution and adapting drive circuits [23]. Segmental structures offer distinct advantages over conventional SRM designs, especially in terms of energy efficiency and flexibility in drive optimization. This extensive research has contributed to the advancement of SRMs in areas such as magnetic circuit optimization, flux routing methods and drive control strategies, and their positioning as an alternative for industrial applications targeting higher efficiency and performance.

In this paper, an innovative control system incorporating a Proportional Integral (PI) control algorithm for a segmental SRM with a 5-phase-10/8 pole configuration is designed and presented. This design incorporates an optimized PI control strategy to provide efficient control of a bipolar-excited segmental rotor SRM. This control algorithm aims to minimize torque fluctuations and increase energy efficiency while significantly improving the dynamic operating performance of the motor.

The study also examines the design details of the driver circuit integrated with the motor's PI control. This driver circuit is capable of effectively managing the magnetic flux variations and phase transitions specific to the segmental rotor structure. A user-friendly computer-based monitoring and control interface has also been developed. This interface allows real-time monitoring of the motor's operating states and easy optimisation of control parameters. The proposed PI control system for the bipolar-excited ST-SRM has been developed to improve the overall operating performance of the motor and optimise energy savings. This design is proposed to be an effective and innovative solution, especially for industrial applications and systems that require high precision.

2. Structural Features of 5-Phase 10/8 Switched Reluctance Motor with Segmental Rotor with Bipolar Excitation

In this section, the structural features of the newly designed segmental-type switched reluctance motor are discussed. Figure 2.1 (a) illustrates the cross-sectional view of the conventional SRM with 5-phase-10/8 pole configuration. Figure 2.1 (b) illustrates the flux paths when the D phase of the conventional SRM is energized in order to compare the performance of the new ST-SRM with bipolar excitation and short magnetic flux paths.

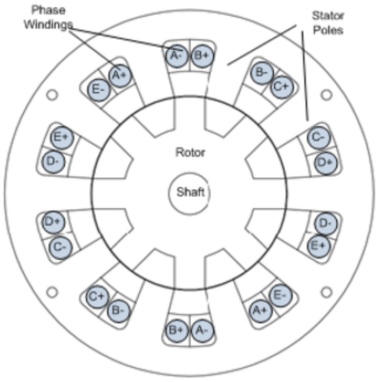

(a) Cross-sectional representation of classical SRM

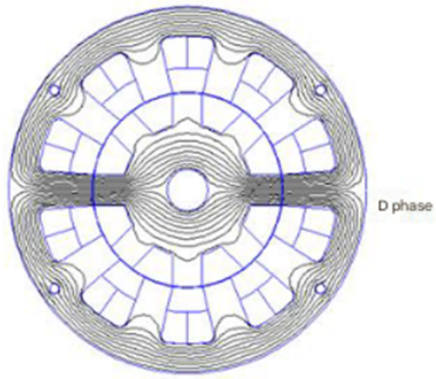

(b) The state of the flux paths in the 5 Phase Classical SRM when only D phase is energised

Figure 2.1: The provides a cross-sectional view of the classical SRM, as well as the of the flux path when one phase is energized

Figure 2.2 shows the new design ST-SRM with 5-phase 10/8 configuration whose design details are expressed. The new developments obtained from ST-SRM can be summarized as follows. ST-SRM with a 10/8 configuration possesses a distinct rotor structure in comparison to the conventional SRM. The rotor comprises silicon steel sheets and an aluminum block, within which these packages are situated. The utilization of an aluminum block is motivated by its capacity to restrict the magnetic field, and its significantly lower density compared to alternative metals such as stainless steel [25].

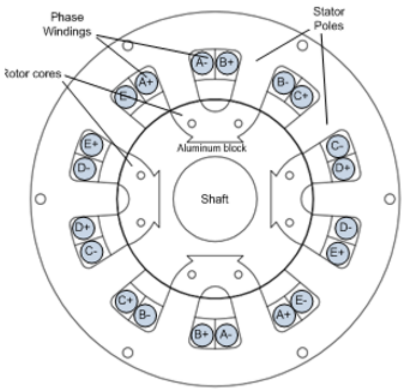

(a) The new ST-SRM is represented in a cross-sectional manner

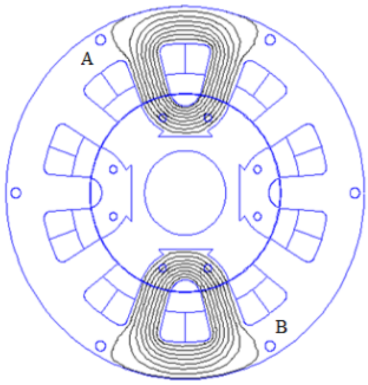

(b) In such a way that only phases A and B form the appropriate polarity the state of the flux paths formed in the new ST-SRM when energized

Figure 2.2: The cross-sectional view of the ST-SRM and the flux path with the phases energized

It is thus evident that the torque value produced per Nm/kg weight, which is a critical factor in the operation of motors, will undergo an automatic increase. In contrast to the single-phase energization method employed in classical SRM, the ST-SRM utilizes a two-phase energization method. The rationale behind this choice is that when the windings are appropriately positioned, and both phases of the ST-SRM are energized concurrently, the magnetic poles of the motor are observed to follow short flux paths. This phenomenon results in a reduction in both the sheet losses and the temperature of the motor sheets. The optimizations have resulted in an enhancement of up to 2.10 times the torque value produced in the motor. Figure 2.2 (b) illustrates that, in contrast to the conventional SRM, the ST-SRM functions through short flux paths rather than long flux paths. It is evident that, given the perpetual energization of two phases, there will be a prevailing common inductance between them, which in turn introduces a degree of complexity to the nonlinear modeling of the motor.

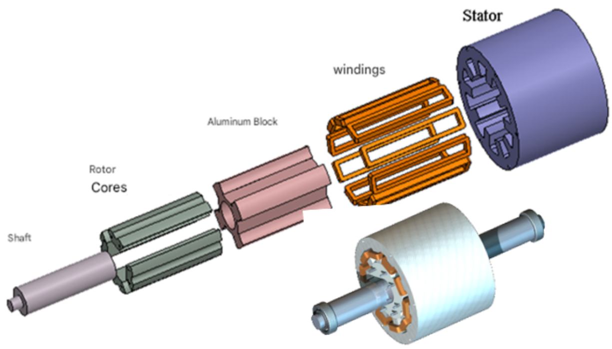

Figure 2.3: New design 5-phase segmental type SRM (ST-SRM) solid view

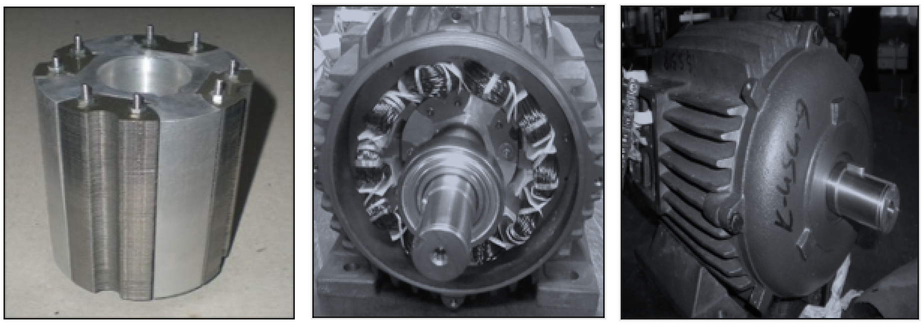

(a) (b) (c)

Figure 2.4: Fabricated machine parts, (a) Rotor (b) Stator (c) Prototype ST-SRM assembly

The advantages of the ST-SRM [25], the design of which has been previously conducted and documented, and whose constituent parts during the production phase are illustrated in Figure 2.4 and whose structural and physical properties are enumerated in Table 2.1, can be enumerated as follows when compared with classical SRM examples: The simultaneous energization of adjacent phases results in the opposite magnetisation of the stator pole pairs, thus forming a one-way magnetic circuit that includes the yoke portion connecting the adjacent stator poles. This enables the ST-SRM to utilize short flux loops of the motor phases at all times, thereby significantly reducing back iron losses, hysteresis and eddy current losses. A notable advantage of the motor is its capability to deliver high torque without the presence of dead torque position, attributable to its low torque ripple characteristic. Consequently, the motor's efficiency is enhanced. The motor is characterized by an air gap that extends along the length of the package, a feature that facilitates more effective cooling by enhancing the thermal management of the motor. Moreover, the ST-SRM's operation on the principle of energizing adjacent poles results in the elimination of secondary magnetic circuits that induce flux switching frequency.

Design Parameter	**Value**
Number of phases	5
Stator/rotor configuration	10/8
Stator outer diameter (mm)	150 mm
Rotor outer diameter (mm)	79.4 mm
Engine yoke (mm)	120 mm
Air gap length	0.3 mm
Stator pole angle (rad)	0.314 rad
Rotor pole angle (rad)	0.331 rad
Number of turns per phase	100
Stator/rotor material	M530-50A silicon steel (0.5 mm thick)
Copper wire diameter (mm)	1.25
Winding resistance per phase (Ω)	0.56
Maximum phase inductance (mH)	67.91

Table 2.1: Structural and physical properties of the prototype ST-SRM

2.1. Mathematical model of ST-SRM

In the classification of electrical machines, mathematical models are generally presented to facilitate a more profound comprehension of the motor-generator operating conditions, to accurately conclude experimental and/or simulation applications, and to identify permanent solutions to problems such as faults and malfunctions. In this section, the mathematical model of the motor and its controller is presented, based on the ST-SRM study employed as a 5-phase model and utilizing the fundamental motor equations. As illustrated in Figure 2.5, the magnetic equivalent circuit of the 5-phase ST-SRM reveals the unique characteristics of this model. A notable distinction from the conventional SRM structure is the direction of flux flow. In the ST-SRM, the flux does not pass from the stator pole to the rotor pole through the air gap, as seen in the classical SRM. Instead, the flux reaches the aluminum block surface on the front surface of the rotor pole through the air gap. This results in a shorter flux path in the ST-SRM. The working principle of the classical SRM is based on the reluctance force, i.e. the force that the rotor experiences when an external force is applied to the position where the flux in the magnetic circuit in which it is located can find the easiest way, where the reluctance is the smallest.

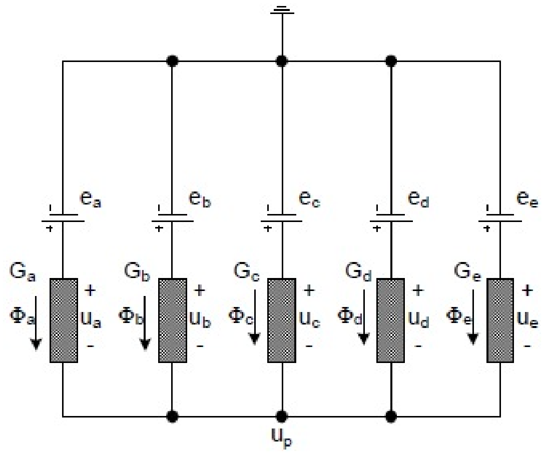

Figure 2.5: Magnetic equivalent of ST-SRM

In accordance with the basic equations of SRM in the classical structure, the torque value produced by the motor is written according to the linear flux model and taking into account the angular change depending on the changing kinetic energy, as shown in the equation below:

$$T(\theta,i) = -\frac{\partial W_c(\theta,i)}{\partial \theta} \quad (\lambda = \text{constant}) \tag{2.1}$$

When the torque generated by the ST-SRM using the expression of Equation (2.1) is calculated using the equivalent circuit model and the phases of each phase of the motor;

$$T = \frac{1}{2}\left(\frac{dL_{aa}}{d\theta}i_a^2 + \frac{dL_{bb}}{d\theta}i_b^2 + \frac{dL_{cc}}{d\theta}i_c^2 + \frac{dL_{dd}}{d\theta}i_d^2 + \frac{dL_{ee}}{d\theta}i_e^2\right) + i_a i_b\frac{dM_{ab}}{d\theta} + i_a i_c\frac{dM_{ac}}{d\theta} + i_a i_d\frac{dM_{ad}}{d\theta} + i_a i_e\frac{dM_{ae}}{d\theta}$$

$$+ i_b i_c\frac{dM_{bc}}{d\theta} + i_b i_d\frac{dM_{bd}}{d\theta} + i_b i_e\frac{dM_{be}}{d\theta} + i_c i_d\frac{dM_{cd}}{d\theta} + i_c i_e\frac{dM_{ce}}{d\theta} + i_d i_e\frac{dM_{de}}{d\theta} \tag{2.2}$$

is obtained. In the given equation (2.2), T is defined as the generated torque (N·m), L is expressed as the inductance of the phase of the coincident position (mH), θ is represented as the angle of rotor position (degrees), M is represented as the mutual inductance (mH) and is defined as the phase current (Amper).
In accordance with Kirshof's flux rule, the subsequent equation can be expressed in its general form:

$$\varphi_a + \varphi_b + \varphi_c + \varphi_d + \varphi_e = 0 \tag{2.3}$$

Phase fluxes are denoted by $\varnothing_x = (x = a,b,c,d,e)$. The flux variation values of each phase are expressed as in the equation below depending on the magnetic conductivity:

$$\varphi_x = G_x(\theta)\,u_x$$

In this context, G_x signifies the magnetic permeability of the phases, with u_x representing the voltage drop. The values of the sources are also calculated according to the equation in the following expression:

$$e_x = N\,i_x \tag{2.4}$$

In equation (2.4), $e_x N$ denotes the value of the opposite electromotive force produced by the source for each phase, N signifies the number of windings for each phase and i_x represents the current of the phases. If u_p is regarded as the mmk value of the potential, the expression;

$$u_x = e_x - u_p$$

is derived. It is possible to calculate the phase fluxes from this extended equation by following the subsequent equation:

$$\varphi_x = G_x(\theta)\,(e_x - u_p).$$

Given that the flux relations of all phases of the ST-SRM model are expressed by $\lambda_x = N\,\varphi_x$,the flux expression of each phase is written as in equation using equation (2.3) for the flux relation.

$$\lambda_a + \lambda_b + \lambda_c + \lambda_d + \lambda_e = 0 \tag{2.5}$$

In the event of the magnetic permeability of each phase being considered as a function of the inductance's of said phases, the result will be;

$$G_x = \frac{L_x}{N^2} \tag{2.6}$$

The expansion of the flux relations of the phases, as outlined in equation (2.6), yields the results;

$$\lambda_x = L_x(\theta)\,\frac{e_x - u_p}{N}$$

If an arbitrary current is defined to be $i_p = \dfrac{u_p}{N}$;

$$\lambda_x = L_x(\theta)\,(i_x - i_p) \tag{2.7}$$

expression is obtained. If this expression we have found is substituted in equation (2.5);

$$L_a(\theta)(i_a - i_p) + L_b(\theta)(i_b - i_p) + L_x(\theta)(i_x - i_p) + L_c(\theta)(i_c - i_p) + L_d(\theta)(i_d - i_p) + L_e(\theta)(i_e - i_p) = 0$$

is obtained. The value of i_p is to be subtracted from the given equation in order to arrive at;

$$i_p = \frac{L_a(\theta)\,i_a + L_b(\theta)\,i_b + L_c(\theta)\,i_c + L_d(\theta)\,i_d + L_e(\theta)\,i_e}{L_a(\theta) + L_b(\theta) + L_c(\theta) + L_d(\theta) + L_e(\theta)}$$

Subsequently, when (2.6) is rearranged according to (2.7), the following is obtained, which corresponds to the flux value for phase A of the ST-SRM:

$$\lambda_a = \left(L_a(\theta) - \frac{L_a^2(\theta)}{L_a(\theta) + L_b(\theta) + L_c(\theta) + L_d(\theta) + L_e(\theta)}\right) i_a - \frac{L_a(\theta)L_b(\theta)\,i_b + L_a(\theta)L_c(\theta)\,i_c + L_a(\theta)L_d(\theta)\,i_d + L_a(\theta)L_e(\theta)\,i_e}{L_a(\theta) + L_b(\theta) + L_c(\theta) + L_d(\theta) + L_e(\theta)} \tag{2.8}$$

The same expression can be written for the other phases by obtaining the same conditions. As can be easily understood from equation (2.8), the self-inductance value for phase A is:

$$L_{aa} = L_a(\theta) - \frac{L_a^2(\theta)}{L_a(\theta) + L_b(\theta) + L_c(\theta) + L_d(\theta) + L_e(\theta)} \tag{2.9}$$

Assuming that the ST-SRM is energized only for the adjacent phases A and B, the inductance value between these phases is found using equation (2.9). In a similar manner, the common inductance values are obtained between the A and B phases as indicated in the equation below:

$$M_{ab} = -\frac{L_a(\theta)\,L_b(\theta)}{L_a(\theta) + L_b(\theta) + L_c(\theta) + L_d(\theta) + L_e(\theta)} \tag{2.10}$$

is obtained.
Common inductance values between other phases can also be expressed using the same mathematical expression, with consideration given to the adjacent phases.

2.2. Apparent Armour profile of ST-SRM

In order to comprehend the study in question more fully, it is first necessary to obtain the apparent inductance profiles for ST-SRM. The values of the apparent inductance are thus found by revealing the states of the different phases at each moment, with the assumption that these phases are driven by an ideal current source. Figure 2.6 (a) shows the connection of the phases as a star, with the phase resistances being neglected due to the calculation method.
As illustrated in Table 2.2, the conditions under which the phases will operate in conjunction for any duration of the SRM utilized as a model are delineated. Consequently, if it is posited that solely the B and C phases are driven in the SRM at the initial moment, the circuit in Figure 2.6 (b) will be obtained. Concurrently, in its most fundamental form, the equivalent circuit is obtained as depicted in Figure 2.6 (c).

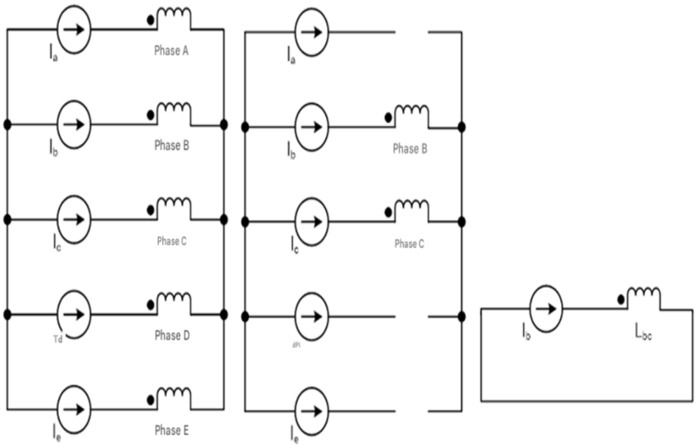

(a) (b) (c)

Figure 2.6: (a) Equivalent circuit of ST-SRM using ideal current sources, (b) State of the equivalent circuit when only phases B and C are energized, (c) Electrical equivalent circuit for phases B and C

Phases	$0^\circ-18^\circ$	$18^\circ-36^\circ$	$36^\circ-54^\circ$	$54^\circ-72^\circ$	$72^\circ-90^\circ$
A Phase	0	+	0	0	−
B Phase	0	0	−	0	+
C Phase	−	0	+	0	0
D Phase	+	0	0	−	0
E Phase	0	−	0	+	0

Table 2.2: Phase operating intervals and corresponding states

Model ST-SRM with B and C phases driven by an ideal current source;

$$i_b = -i_c, \quad i_a = 0, \quad i_d = 0, \quad i_e = 0$$

group of equations can be obtained. The flux relations for this energization state can be found and expressed separately for λ_b and λ_c. We can express it by finding it separately for each phase. The path followed by the flux; Since the value of the flux passing through the air gap of phase B to phase C is $\lambda_{ab} = \lambda_a - \lambda_b$;

$$\lambda_{bc} = \left[L_b(\theta) + L_c(\theta) - \frac{L_b^2(\theta) + L_c^2(\theta)}{L_a(\theta) + L_b(\theta) + L_c(\theta) + L_d(\theta) + L_e(\theta)} + \frac{2L_b(\theta)L_c(\theta)}{L_a(\theta) + L_b(\theta) + L_c(\theta) + L_d(\theta) + L_e(\theta)} \right] i_b$$

expression is obtained. The apparent inductance value, denoted by L_{bc}, is calculated by substituting this value into the equation $L = \frac{\lambda}{i}$, utilising the flux expression that has been previously defined. The expression obtained in the equation below is the common inductance equation between phases B and C.

$$L_{bc} = L_b(\theta) + L_c(\theta) - \frac{L_b^2(\theta) + L_c^2(\theta)}{L_a(\theta) + L_b(\theta) + L_c(\theta) + L_d(\theta) + L_e(\theta)} + \frac{2L_b(\theta)L_c(\theta)}{L_a(\theta) + L_b(\theta) + L_c(\theta) + L_d(\theta) + L_e(\theta)}.$$

3. Design of Drive Circuit with PI Control for Bipolar Driven ST-SRM

In this section, an innovative driver circuit developed for the control of a bipolar-driven ST-SRM incorporating a PI control algorithm is discussed. The driver circuit is designed to consist of two main parts. The first part is configured to drive only the phase windings, which are designed as 5-phase. The second part is a control mechanism that runs the PI control algorithm and dynamically adjusts the source voltage according to the current requirements by continuously monitoring the system's real-time performance. Due to this structure, the efficiency and performance of the motor are increased by rapidly adapting to the operating conditions of the system. Two separate microprocessor subsystems are used to realize these features of the circuit. This dual microprocessor architecture enables the implementation of complex control algorithms in a more robust framework, especially in bipolar-driven circuits. This design approach significantly improves the efficiency of ST-SRM by increasing the stability and sensitivity of the motor.

3.1. The system that drives the PI controller

In this driver circuit, based on the speed information obtained from the ends of the ST-SRM through optical sensors, a driver circuit has been developed that can dynamically increase and decrease the bus voltage in accordance with the current requirements of the motor. This innovative system is designed to optimise motor performance and improve energy efficiency.
The developed system consists of three basic layers:

1. **Supply circuit:** It is the layer that provides the necessary energy to the system and regulates the voltage level.

2. **PIC control circuit:** It is the control unit that processes the speed information from the optical sensors and determines the voltage level required by the motor by running the PI algorithm.
3. **MOSFET driver stage:** It is the unit that realises the power transfer to the motor phases by increasing or decreasing the bus voltage in accordance with the signals received from the control circuit.

Before explaining the steps to be followed for the implementation of the PI algorithm, it is important to examine the flowchart of the system given in Figure 3.1 and the actual image of the drive circuit. These visualisations will allow a clearer understanding of the overall structure and operation of the system.

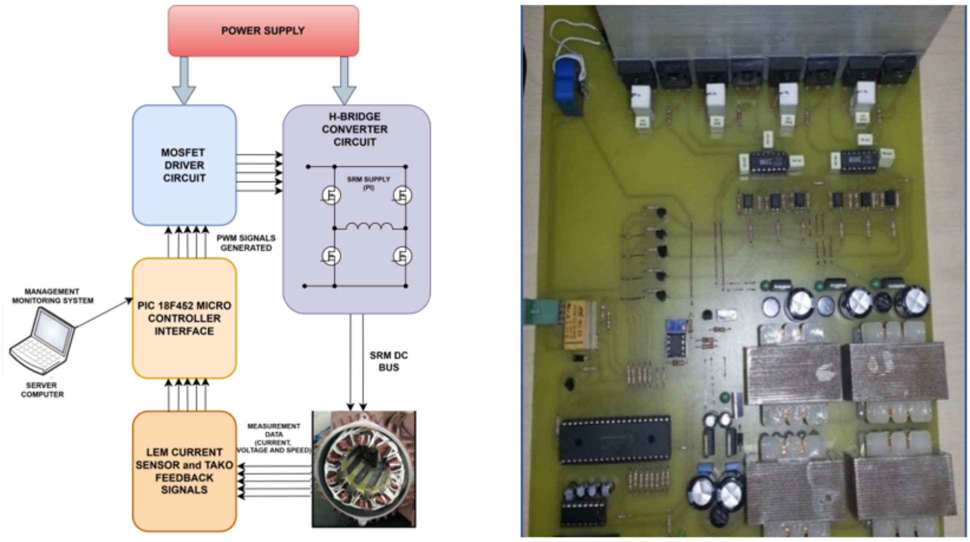

Figure 3.1: Flowchart of the circuit performing the PI algorithm and the circuit image where the PI algorithm is executed

A Proportional Integral (PI) controller is used to reduce or increase the bar tension according to the current requirement arising depending on the information of speed read through the optical sensors from the ends of SRM with a segmental structure driven in this circuit. Nowadays, the most of controllers are implemented by computer algorithms [20]. The linear part of a classical PI controller with amplitude of the current command can be formalized where K_p is the proportional control gain, K_i is the integral control gain, and i^* is the amplitude of the current command. The position sensor senses the rotor position, and the motor speed (ω) is given by the derivative of the rotor position information. In the PI controller, the speed error calculates (ω_{ce}) from the difference between the motor speed and the set reference speed (ω^*).

$$i^* = K_p(\omega^* - \omega) + K_i \int (\omega^* - \omega)\, dt$$

The speed error (ω_e) and change in speed error (ω_{ce}) as input variables at k-th sampling instant is given by

$$\omega_e(k) = \omega^* - \omega(k)$$

$$\omega_{ce}(k) = \omega_e(k) - \omega_e(k-1)$$

The torque signal T_e^*, which is fed to the reference current, is the output of the PI speed controller. The variable of controller output is the change in reference current $\Delta i^*(k)$. A computer implementation of a PI controller can be analysed as a difference equation.

$$i^*(k) = i^*(k-1) + \Delta i^*(k)$$

$$i^*(k) = i^*(k-1) + K_i\, \omega_e(k) + K_p\, \omega_{ce}(k)$$

The values of K_p and K_i relate the parameters of the drive system. The conventional pole placement technique is not necessarily to lead optimum stable the complex control structure of the SRM. Therefore, the controller gains are selected by comparing the effects of K_p and K_i on the speed response of the drive. In this application, feedback signals are given the rotor position θ and the phase currents i_a, i_b, i_c, i_d, i_e, and the speed is calculated by the rotor position signal. Turn-On angle θ_{on}, Turn-Off angle θ_{off}, and pulse width modulation duty cycle are controlled by the switching signal generator [26].
In accordance with the general flowchart and circuit image presented in Figure 3.1, the hardware employed for PI control of ST-SRM can be enumerated as follows:

- **Supply circuit:** It is designed as a 4 transformer power supply circuit that can operate between ± 5 V and ± 15 V, fed from a 220 V, 10 A power supply.
- **Programming and control circuit:** The circuit that enables the implementation of the control algorithms is realised with the PIC18F452 microcontroller.

- **Management and monitoring system:** Provides monitoring and management of real-time data (current, power, speed, etc.) of the system.
- **RS232 communication protocol:** This is the interface that performs data communication between the system and the computer.
- **MOSFET driver circuit:** This is designed using IR2110 MOSFET driver integral.

It is a well-established fact that all equipment utilised in the domain of PI driver circuit design typically functions with a supply voltage that falls within the range of 5V-15V. This supply is facilitated by a bespoke power supply circuit comprising four layers.
The programming and measurement circuits are designed with the aid of a PIC18F452 microcontroller, with variables such as current, power, and speed obtained during system operation being transmitted to a computer and monitored via the RS232 communication protocol. Concurrently, the microcontroller manages the MOSFET drivers in accordance with the computer's commands and drives IRFP250-type MOSFETs. The measurement circuits, in conjunction with the LEM current sensor, detect signals from a tachogenerator connected to the ARM shaft, generating a voltage of 2.5 V at 1000 rpm, depending on the motor speed.
The MOSFET driver and converter circuit have been designed using optical transistors and IR2110-type MOSFET drivers. The function of this circuit is to process the Pulse Width Modulation (PWM) drive signals from the PIC18F452 microcontroller and switch IRFP250 type MOSFETs into conduction. Furthermore, it is able to dynamically adjust the DC bus voltage to which the motor is connected according to the current requirement by running the PI algorithm. This configuration has been shown to enhance the performance of the system and optimise energy efficiency.

3.2. ST-SRM drive control interface

The interface displayed in Figure 3.2 has been designed to monitor faults that may occur in the phases of the motor during operation, as well as to monitor the motor speed instantaneously depending on time. In accordance with the working principle of ST-SRM, although the phase currents can change direction and reach negative values, these values are organised in the interface software so that they are always positive. This approach renders fault monitoring more practical. The interface facilitates the real-time observation of the current drawn by each motor phase from the fields on the left panel, thereby enabling the swift identification of anomalies such as a sudden decline in motor speed. Furthermore, it permits the discernment of the phases energised during start-up and the identification of those drawing higher currents than others. These capabilities underpin the effective analysis of system performance and faults.

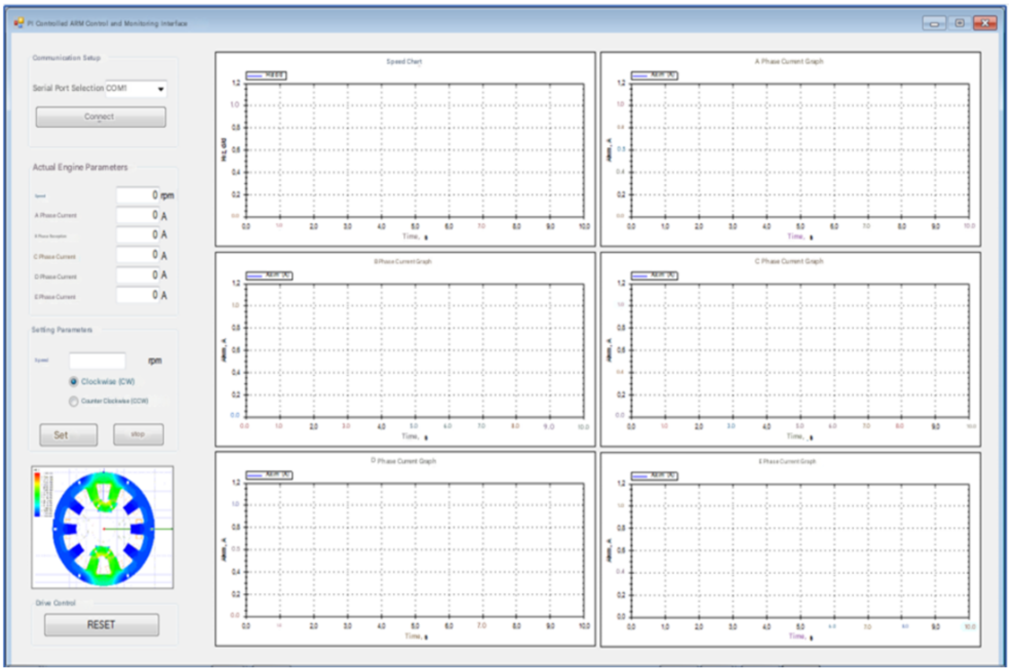

Figure 3.2: ST-SRM control and monitoring interface

The monitoring interface is composed of four primary components:

1. **Communication Settings:** This section, located at the top of the interface, is where system connection and port settings are configured. During the initial connection of the computer to the drive system via a serial port, the USB port employed (e.g. COM1, COM7) must be selected accurately. The successful establishment of the connection can be readily identified by observing the changes in the motor parameters section.
2. **Real Motor Parameters:** This section displays motor phase currents in real-time, with this data being monitorable not only from this window but also from the main monitoring windows.
3. **Setting Values:** This section is where the operating parameters of the motor are set and monitored. From here, rotation commands of the motor can be issued, the speed level can be adjusted, the active status of the drive circuit can be controlled, and the rotation direction of the motor can be changed.
4. **Monitoring Windows:** These windows facilitate the online observation of the speed of the switched reluctance motor and the changes in phase currents over time, thereby providing detailed monitoring of the performance parameters of the motor.

4. Experimental Study and Results

In this section, the focus will be on the experimental studies performed on the PI controlled ST-SRM. Prior to the presentation of the results obtained in the experiments and the subsequent discussion of the differences between these results, it will be beneficial to examine the experimental setup. In addition to the driver circuit and software described in the previous section, the experiments were carried out using some external hardware in the setup shown in Figure 4.1. These external components are detailed through the numbers on the setup.

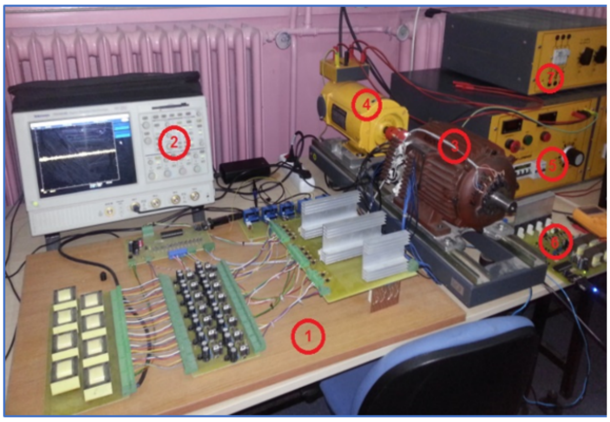

1. ST-SRM 5-phase drive system,

2. 4-channel oscilloscope,

3. 10/8 ST-SRM with 5-phase bipolar excitation,

4. DC generator (120V, 0.55A excitation) coupled to the motor,

5. Power supply (Maximum: 240V, 8A),

6. Driver board realising PI control function,

7. 1 kW regulated resistive load group.

Figure 4.1: ST-SRM Experimental Setup

In addition to the experimental set-up, two personal computer groups have been configured to control and monitor both the PI driver card and the ST-SRM driver system. These groups also perform graphical monitoring of the values in real time
Prior to the presentation of the experimental results on the PI-controlled ST-SRM, it is beneficial to provide a comprehensive review of the operational dynamics of the experimental setup. The system functions in the following manner:

- Following the provision of power to the circuit, the driver cards are connected via a serial port.
- Activation of the driver card responsible for driving the ST-SRM is initiated through the interface, with the control of data flow occurring from the screen.
- Upon the connection of the PI control card and the augmentation of voltage from the regulated power supply, an observation is made of the acceleration of the motor. In the absence of such an observation, the possibility of a fault in the connection cards is a consideration.

4.1. PI controller experiments with ST-SRM loaded state

The most critical point in monitoring the operating regime of switched reluctance motors is to follow the time-dependent current changes. The current curves presented in Figure 4.2 (a) and (b) clearly show that the observed fluctuations of the motor under load are an important indicator for evaluating the efficiency of the driver circuit.

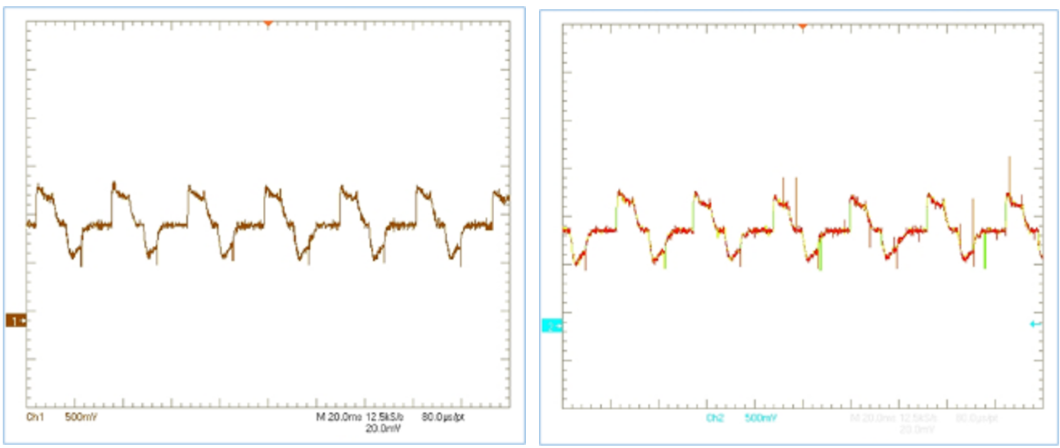

(a) (b)

Figure 4.2: (a) Time-dependent variation of the current of phase A measured from channel 1 under loaded condition (b) Time-dependent variation of phase B current measured from channel 2 under loaded condition

A fundamental aspect of operating SRMs is the capacity to monitor time-varying currents, as evidenced by the analysis of the current curves depicted in Figure 4.2 (a) and (b). It is noteworthy that the current curves obtained in real-time closely resemble those derived from simulations, underscoring the significance of fluctuations, particularly in motor loading conditions, in assessing the efficiency of the drive circuit. Furthermore, the values obtained between Figure 4.3 and Figure 4.7 for the operating regime of the ST-SRM were obtained for the interfaces introduced here and realized for the PI-controlled driver circuit.

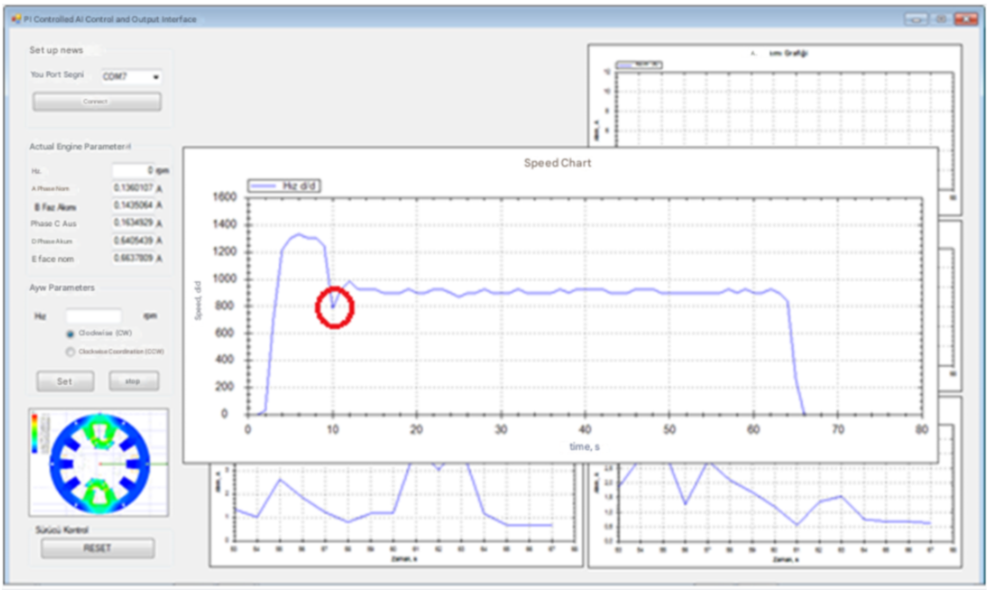

Figure 4.3: ST-SRM Experimental Setup

As illustrated in Figure 4.3, in the operating case under consideration, the ST-SRM is initially run in an idle state (at a speed of approximately 1300 rpm) and the PI controller is activated at the 10th second. At this point, the real-time response of the controller (K_p=15, K_i=350) can be readily observed through the red-coloured area. The primary objective of the experiment is to maintain a constant motor speed of 900 rpm, a feat that is readily apparent in the demonstration of the efficacy of the PI controller in ensuring the motor speed remains at the target value

In consideration of the present variation, the present data cannot be monitored in real-time as in the oscilloscope due to the utilization of PIC in the driver circuit and the preference of serial port control for data transfer. Since the data is collected at one-second intervals, an irregular distribution can be observed. The interface developed for this study aims to monitor faults occurring in the motor phases in a time-dependent manner. The software facilitates fault tracing by showing these data as positive when the phase currents change direction or reach negative values. Additionally, the interface enables real-time monitoring of the current drawn by each phase, a feature that is instrumental in conducting reliable and performance-oriented analyses of the system.

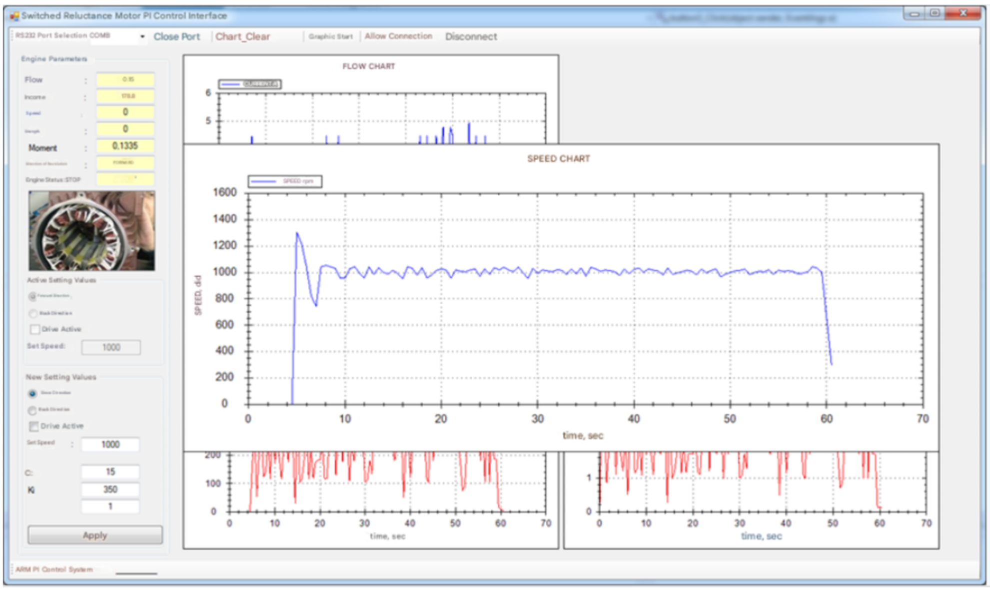

Figure 4.4: Change obtained on the PI control side of ST-SRM

In this experiment, the speed of the motor was maintained at 1000 rpm. Upon examination of the motor parameters via the interface depicted in Figure 4.4, it was observed that a voltage value of 178 V could not be identified in relation to the voltage value of the motor. This is a parameter associated with the PWM increase and the proportion of PWM applied to the motor terminals.

4.2. ST-SRM Fixed Load and Variable Speed PI Controller Experiments

In this particular instance of ST-SRM, the motor load was maintained at a constant level, while the amplitude of the PWM signal was modified by establishing the motor voltage at 40 V. As illustrated in Figure 4.5 (a) and Figure 4.5 (b), the temporal variations in the motor currents were observed. Subsequently, the alterations in the motor on the controller and PI control sides are depicted in Figure 4.6 and Figure 4.7, respectively.

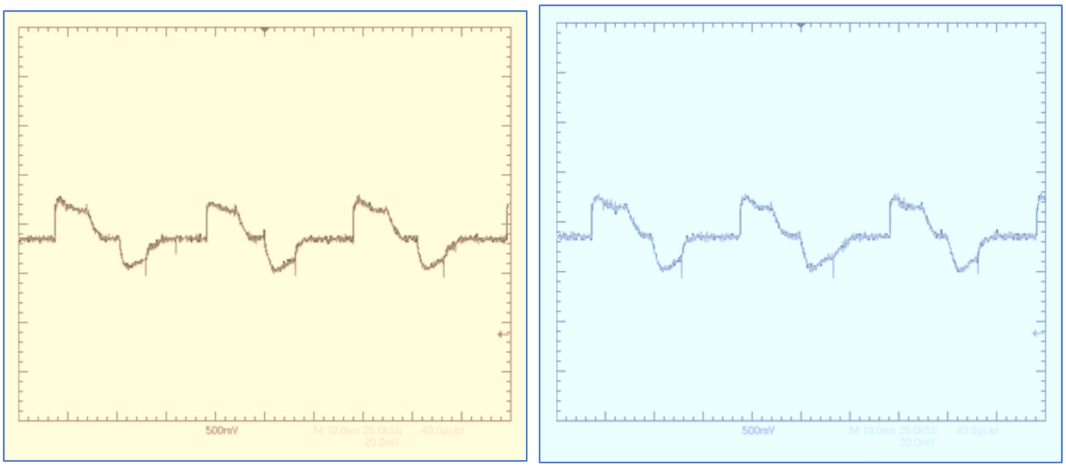

(a) (b)

Figure 4.5: (a) Time-dependent variation of C phase current when ST-SRM is loaded (b) Time-dependent variation of D phase current when ST-SRM is loaded

Figure 4.6: Time-dependent speed and current changes of the controller side of ST-SRM

A thorough examination of the graphs in Figure 4.6 and Figure 4.7 reveals that the motor speed increases to 400 rpm, 600 rpm, 800 rpm, 1000 rpm. This sequence is repeated, with the motor speed increasing to 800 rpm, then decreasing to 600 rpm, and then increasing again to 1000 rpm. The motor speed then remains constant at 1000 rpm, due to the changes in the PWM signal, while the ST-SRM load remains constant. The speed graph effectively shows the response of the PI controller to the transitions at each speed level. It is observed that the PI controller reduces the speed deviations and ensures a stable reaching of the target speed value.

The graphical representation of the current, speed, power, and torque changes obtained in real-time provides satisfactory results in terms of evaluating the dynamic performance of the system, with the speed graph revealing the rapid adaptation of the PI controller to instantaneous changes and its success in ensuring that the system reaches the target speed value. These results make it possible to make a positive evaluation in terms of the reliability of the system and the effectiveness of the control algorithm.

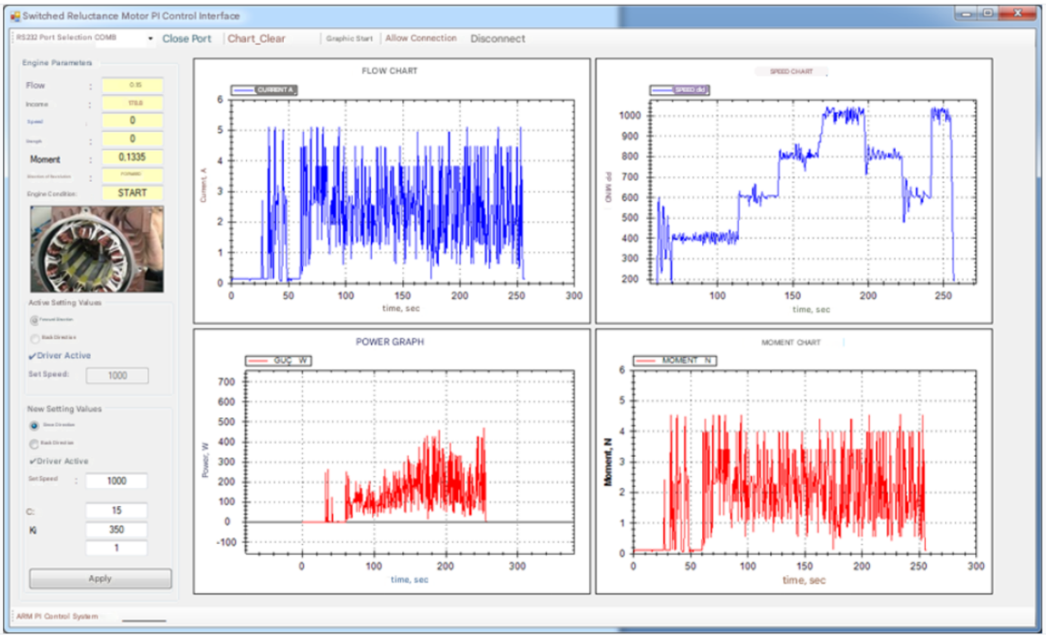

Figure 4.7: Time dependent bus current, speed, consumed power and torque variations of the PI controller side of ST-SRM

5. Conclusion

In recent years, considerable research and studies have been conducted on switching reluctance motors, particularly with regard to driving methods. The present study proposes a PI-controlled drive and monitoring system for speed and load control of a novel ST-SRM with a 5-phase, 10/8 pole configuration, and bipolar excitation. The theoretical underpinnings are substantiated by deriving the equations of state for a previously prototyped ST-SRM.

The development of a driver system with four main components, comprising a power stage, a control circuit, a converter, and a PI control stage, has been achieved. The integration of the designed driver circuit with the converter circuit has been accomplished, resulting in enhanced system integrity and streamlined design. Following the completion of the design and prototype development stages of the driver circuit system, experimental studies were initiated. The developed user interface provided the opportunity to monitor the motor's time-dependent speed, voltage, and current changes instantaneously and, at the same time, facilitated motor control for the user. This study has made a significant contribution to the control and monitoring systems of segmental rotor-switched reluctance motors and increased their application potential.

Future studies can focus on optimising PI control algorithms and further improving the performance of the system by applying alternative control methods such as adaptive control and artificial intelligence-based algorithms on ST-SRMs. Furthermore, research on how the segmental rotor structure can be adapted for different motor configurations and application areas can enable the integration of the motor into wider industrial areas. Such developments will further expand the efficiency and application areas of segmental rotor SRMs.

Article Information

Acknowledgements: The author would like to express his sincere thanks to the editor and the anonymous reviewers for their helpful comments and suggestions.

Conflict of Interest Disclosure: No potential conflict of interest was declared by the author.

Plagiarism Statement: This article was scanned by the plagiarism program.

References

[1] T. J. E. Miller, *Switched Reluctance Motors and Their Control*, Oxford Science Publications, 2018.
[2] P. J. Lawrenson, J. M. Stephenson, P. T. Blenkinsop, et al., *Variable-speed switched reluctance motors,* IEE Proc. B Electr. Power Appl., **127** (4) (1980), 253–265. https://doi.org/10.1049/ip-b.1980.0034
[3] R. Krishnan, *Switched Reluctance Motor Drives: Modelling, Simulation, Analysis, Design, and Applications*, CRC Press, 2001.
[4] M. A. Patel, K. Asad, Z. Patel, et al., *Design and optimisation of slotted stator tooth switched reluctance motor for torque enhancement for electric vehicle applications*, Int. J. Ambient Energy, **43**(1) (2021), 4283–4288.
[5] K. Diao, X. Sun, G. Bramerdorfer, et al., *Design optimisation of switched reluctance machines for performance and reliability enhancements: A review*, Renew. Sustain. Energy Rev., **168** (2022), Article 112785.
[6] X. Sun, X. Tang, X. Tian, et al., *Sensorless control with Fault-Tolerant ability for switched reluctance motors*, IEEE Trans. Energy Convers., **37**(2) (2022), 1272–1281.
[7] M. Omar, E. Sayed, M. Abdalmagid, et al., *Review of machine learning applications to the modelling and design optimisation of switched reluctance motors*, IEEE Access, **10** (2022), 130444–130468.
[8] K. Vijayakumar, R. Karthikeyan, S. Paramasivam, et al., *Switched reluctance motor modelling, design, simulation, and analysis: A comprehensive review*, IEEE Trans. Magn., **44**(12) (2008), 4605–4617.
[9] Z. Xu, T. Li, F. Zhang, et al., *A review on segmented switched reluctance motors*, Energies, **15**(23) (2022), 9212.

[10] A. Peniak, J. Makarovic, P. Rafajdus, et al., *Design and optimisation of switched reluctance motor for electrical vehicles*, Electr. Eng., **99** (2017), 1393–1401.
[11] X. Gao, R. Na, C. Jia, et al., *Multi-objective optimisation of switched reluctance motor drive in electric vehicles*, Comput. Electr. Eng., **70** (2018), 914–930.
[12] M. Tursini, M. Villani, G. Fabri, et al., *A switched-reluctance motor for aerospace application: Design, analysis and results*, Electr. Power Syst. Res., **142** (2017), 74–83.
[13] R. Krishnan, *An energy-efficiency-enhanced switched reluctance motor [From Mind to Market]*, IEEE Ind. Electron. Mag., **1**(1) (2007), 4–6.
[14] S. K. Sahoo, S. K. Panda, J. X. Xu, *Iterative learning-based high-performance current controller for switched reluctance motors*, IEEE Trans. Energy Convers., **19**(3) (2004), 491–498.
[15] Z. Touati, M. Pereira, R. E. Araújo, et al., *Integration of switched reluctance generator in a wind energy conversion system: An overview of the state of the art and challenges*, Energies, **15**(13) (2022), 4743.
[16] B. Bilgin, J. W. Jiang, A. Emadi, *Switched Reluctance Motor Drives: Fundamentals to Applications*, CRC Press, Boca Raton, FL, 2018.
[17] R. M. Pindoriya, B. S. Rajpurohit, R. Kumar, et al., *Comparative analysis of permanent magnet motors and switched reluctance motors capabilities for electric and hybrid electric vehicles*, Proceedings of the 2018 IEEMA Engineer Infinite Conference (eTechNxT) (2018), 1–5.
[18] L. Feng, X. Sun, G. Bramerdorfer, et al., *A review on control techniques of switched reluctance motors for performance improvement*, Renew. Sustain. Energy Rev., **199** (2024), Article 114454.
[19] E. Büyükbıçakcı, A. F. Boz, *Examination of state equations and dynamic simulation results of a new type 5-phase switched reluctance motor with a segmental rotor*, Kirklareli Univ. J. Eng. Sci., **7**(2) (2021), 232–256.
[20] D. Uygun, G. Bal, *Linear model of a novel 5-phase segment type switched reluctance motor*, Electron. Electr., **20**(3) (2014), 3–7.
[21] P. J. Lawrenson, L. Agu, *Development of reluctance motors for Industrial Applications*, Proceedings of the Institution of Electrical Engineers, **111**(3) (1964), 243–251.
[22] A. G. Jack, B. C. Mecrow, J. A. Haylock, *A Comparative study of permanent magnet and switched reluctance motors for high-performance Fault-Tolerant applications*, IEEE Trans. Ind. Appl., **32**(4) (1996), 889–895.
[23] V. S. Murty, S. Jain, A. Ojha, *Analyzing modeled configuration using finite element analysis for performance prediction of LSRM*, Neural Comput. Appl., **34** (2022), 21175–21189.
[24] J. Cai, B. Li, A. D. Cheok, et al., *Optimal design and control of a decoupled multi-frequency multi-phase wireless switched reluctance motor drive system*, IEEE Trans. Power Electron., **39**(8) (2024), 10152-10165.
[25] D. Uygun, *Design and application of 5-phase U-type segmental rotor bipolar excitation 10/8 switching reluctance motor*, PhD Thesis, Institute of Science and Technology, Gazi University, Ankara, 2012, 10–15.
[26] Ö. F. Bay, Ç. Elmas, *Modelling of the inductance variation and control of the switched reluctance motor Based on fuzzy logic*, Intell. Autom. Soft Comput., **10**(3) (2004), 233–246.